

Vortex phase diagram for mesoscopic superconducting disks

V.A. Schweigert[†], F.M. Peeters[‡], and P.S. Deo
*Departement Natuurkunde, Universiteit Antwerpen (UIA),
 Universiteitsplein 1, B-2610 Antwerpen, Belgium*
 (November 26, 2017)

Solving numerically the 3D non linear Ginzburg-Landau (GL) equations, we study equilibrium and nonequilibrium phase transitions between different superconducting states of mesoscopic disks which are thinner than the coherence length and the penetration depth. We have found a smooth transition from a multi-vortex superconducting state to a giant vortex state with increasing both the disk thickness and the magnetic field. A vortex phase diagram is obtained which shows, as function of the magnetic field, a re-entrant behavior between the multi-vortex and the giant vortex state.

PACS number(s): 74.24.Ha, 74.60.Ec, 73.20.Dx

Recently, mesoscopic superconductivity has attracted much attention in view of phase transitions in confined systems with sizes comparable to the coherence (ξ) and penetration (λ) lengths. While the type of bulk superconductors is only determined by the value of the Ginzburg-Landau parameter $\kappa = \lambda/\xi$, the experimental observations [1] and the numerical simulations [2,3] of magnetization of mesoscopic thin disks have shown that the *type* and the *order* of those transitions between different superconducting states and between the superconducting and the normal state depends crucially on the disk radius R and the thickness d . With increasing the disk radius the second-order reversible phase transition observed for small disk radii are replaced by first-order transitions with a jump in the magnetization. In previous theoretical investigations of superconductivity in such mesoscopic disks [2,3] only the giant vortex states with fixed total angular momentum L were considered with an axially symmetric order parameter. It is well known [4] that for type-II superconductors ($\kappa > 1/\sqrt{2}$), the triangular Abrikosov vortex lattice is energetically favorable in the range $H_{c1} < H < H_{c2}$. Since the effective London penetration depth $\Lambda = \lambda^2/d$ increases considerably in thin disks with $d \ll \lambda$ one would expect the appearance of the Abrikosov multi-vortex state even in disks made from a material with $\kappa < 1/\sqrt{2}$, like e.g. the *Al* disks studied in Refs. [2,3]. By analogy with classical particles confined by an external potential [5], the structure of a finite number of vortices should differ from a simple triangular arrangement and allow for different metastable states. Using the London approximation Fetter [6] calculated the critical field H_{c1} for flux penetration into a disk. For a superconducting cylinder the multi-vortex clusters, containing up to four vortices, were simulated by Bobel [7]. Using the method of images and the London approximation, Buzdin and Brison

[8] have considered vortex structures in small $R \ll \Lambda$ disks and found a classical particle ringlike arrangement [5] of vortices. In the present Letter we study the transition from the giant vortex state to this multi-vortex configuration for thin superconducting disks within the nonlinear Ginzburg-Landau (GL) theory.

We consider a superconducting disk immersed in an insulator media with a perpendicular uniform magnetic field H_0 . For thin disks ($d \ll \xi, \lambda$) we found [2,3] that it is allowed to average the GL equations over the disk thickness. Using dimensionless variables and the London gauge $div \vec{A} = 0$ for the vector potential \vec{A} , we write the system of GL equations in the following form

$$\left(-i\vec{\nabla}_{2D} - \vec{A}\right)^2 \Psi = \Psi(1 - |\Psi|^2), \quad (1)$$

$$-\Delta_{3D}\vec{A} = \frac{d}{\kappa^2}\delta(z)\vec{j}_{2D}, \quad (2)$$

$$\vec{j}_{2D} = \frac{1}{2i}\left(\Psi^*\vec{\nabla}_{2D}\Psi - \Psi\vec{\nabla}_{2D}\Psi^*\right) - |\Psi|^2\vec{A}, \quad (3)$$

with the boundary condition $(-i\vec{\nabla}_{2D} - \vec{A})\Psi|_{r=R} = 0$. Here the distance is measured in units of the coherence length ξ , the vector potential in $c\hbar/2e\xi$, and the magnetic field in $H_{c2} = c\hbar/2e\xi^2 = \kappa\sqrt{2}H_c$. The disk is placed in the plane (x, y) , the external magnetic field is directed along the z -axis, the indices $2D, 3D$ refer to two-dimensional and three-dimensional operators, and \vec{j}_{2D} is the density of superconducting current. To solve the system of Eqs.(1-2) we apply a finite-difference representation of the order parameter and the vector potential on a uniform cartesian space grid (x, y) and use the link variable approach [9]. In our simulations we took typically a grid spacing of 0.15ξ . To find the steady-state solution of the GL equations we add to the LHS of Eqs. (1) and (2) the time derivatives of the order parameter and the vector potential, respectively, and use an iteration procedure based on the Gauss-Seidel technique to find Ψ . The vector potential is obtained with the fast Fourier transform technique. For this purpose we set the condition for the vector potential $\vec{A}|_{|x|=R_s, |y|=R_s} = H_0(x, -y)/2$ at the boundary of a larger space grid ($R_s = 4R$), where the vector potential created by the superconducting currents is much less than the external vector potential.

The giant vortex state is characterized by the total angular momentum L through $\Psi = \psi(\rho)\exp(iL\phi)$, where ρ, ϕ are the cylindrical coordinates. An arbitrary superconducting state is generally a mixture of different angular

harmonics. Nevertheless, we can introduce an analog to the total angular momentum which is still a good quantum number. Choosing circular loops at the periphery of the disk we find that the effective angular momentum $L = \Delta\phi/2\pi$ does not depend on the loop radii ρ_l when it is in some range $\rho_l = (0.8 \div 1)R$. This allows us to characterize unambiguously the different superconducting states. Note, that the effective angular momentum is in fact nothing else then the number of vortices in the disk.

To find the different vortex configurations, which include the metastable states, we search for the steady-state solutions of Eqs.(1-2) starting from different initial conditions which were generated randomly. Once we obtained these configurations for some value of the magnetic field we increase/decrease slowly the magnetic field as long as the number of vortices remains unchanged. Comparing the dimensionless Gibbs free energies $F = V^{-1} \int (2(\vec{A} - \vec{A}_0)\vec{j}_{2d} - |\Psi|^4) d\vec{r}$, where integration is performed over the disk volume V , and \vec{A}_0 is the vector potential of the external uniform magnetic field, we found the ground state. If the system has sufficient time to equilibrate, the system will be in the ground state and we obtain phase transitions between different ground states. If the latter condition is not satisfied the system can remain in a metastable state until this state disappears or becomes unstable with respect to small perturbations in the order parameter and/or the magnetic field. Such nonequilibrium phase transitions lead to hysteresis in the magnetization. The barriers separating the metastable and the ground state are discussed in Refs. [10,11]. The system remains in the metastable state if the barrier height is much larger than the temperature. Instead of finding the barrier heights, which is a more cumbersome problem, we search for the critical magnetic fields corresponding to the disappearance of such barriers. Here, we started from the Meissner (normal) state and increased (decreased) slowly the magnetic field (typically with steps of $0.01H_{c2}$) from the zero (nucleation) magnetic field.

The free energies of the different vortex configurations are shown in Fig. 1 for zero disk thickness and for two disk radii: (a) $R = 4\xi$, and (b) $R = 4.8\xi$. For $R = 4\xi$, the vortex configuration can consist up to six vortices which are arranged on the edge of an ideal polygon. The pentagon and hexagon vortex clusters are always metastable states for $R = 4\xi$. With increasing disk radius the allowed number of vortices increases leading to the appearance of polygons with a vortex inside it when $L > 7$. We found that these structures have a larger energy as compared to the ideal polygons. This result differs from the London approximation of Ref. [8] where the vortices were treated as an ensemble of interacting classical point pseudoparticles in which the closed packed structures are more preferable even for $L \geq 6$. The present work clearly shows the limited validity of the approach of Ref. [8] for the case of superconducting disks. Another unexpected

feature is observed when the magnetic field is further increased. While the model of classical particles predicts a decrease in the intervortex distance followed by the appearance of a new vortex, our simulations show, as a rule, a gradual transition from a *multi-vortex state* to a *giant vortex state* (Fig. 2). In principle, the latter may be a metastable state. The positions of these transitions are indicated by circles in Fig. 1. For a larger disk radius $R = 4.8\xi$, we also observe transitions between different multi-vortex states. Performing a Fourier analysis of the order parameter we find that a multi-vortex state corresponding to an ideal polygon presents a mixture of harmonics $\Psi \approx \psi_0(\rho) + \sum_k \psi_k(\rho) \exp(ikL\phi)$ with a rather small contribution of higher ($k > 2$) harmonics. This allows us to find approximately the free energy of different vortex configurations in thin disks $R \ll \Lambda$ in which we can neglect the distortion of the magnetic field. For this purpose we take the order parameter as a superposition of only two states $\Psi \approx C_0^{1/2} \zeta_0(\rho) + C_L^{1/2} \zeta_L(\rho) \exp(iL\phi)$, where ζ_0, ζ_L are the eigenfunction of the linearised first GL equation (1) for different angular momenta [3,12]. Substituting this expansion into Eq.(1) we obtain the following set of non-linear equations for the coefficients C_0 and C_L

$$\begin{aligned} \lambda_0 C_0 &= a_{11} C_0^2 + a_{12} C_0 C_L, \\ \lambda_L C_L &= a_{12} C_0 C_L + a_{22} C_L^2, \end{aligned} \quad (4)$$

with $a_{11} = \langle \zeta_0^2 | \zeta_0^2 \rangle$, $a_{12} = 2 \langle \zeta_0^2 | \zeta_L^2 \rangle$, $a_{22} = \langle \zeta_L^2 | \zeta_L^2 \rangle$, where λ_0, λ_L are the eigenvalues of the linearised GL equation [3], and $\langle f_0 | f_1 \rangle$ refers to the matrix element $V^{-1} \int f_0 f_1 d\vec{r}$. Besides the two trivial solutions $C_L = 0$, $C_0 = \lambda_0/a_{11}$ and $C_0 = 0$, $C_L = \lambda_L/a_{22}$ which correspond to the Meissner state and the giant vortex state, respectively, it is possible to have another solution with $C_0 = (\lambda_0 a_{22} - \lambda_L a_{12})/D$, $C_L = (\lambda_L a_{11} - \lambda_0 a_{12})/D$, $D = a_{11} a_{22} - a_{12}^2$ corresponding to a multi-vortex state. The free energy of the ground state obtained using this approach, is shown in Fig. 1 by the dashed curve, which is in good agreement with the results of our simulations (full curves). In order to discuss the multi-vortex \leftrightarrow giant vortex transition, we analyzed the stability of the obtained solutions with respect to small perturbations of the coefficients C_0, C_L (see Ref. [3]). The stability conditions for the multi-vortex state and the giant vortex state are $\lambda_L < \lambda_* = \lambda_0 a_{22}/a_{12}$ and $\lambda_L > \lambda_*$, respectively. Consequently for fixed L , there is an unique solution with a reversible transition from the multi-vortex state to the giant vortex, which occurs with increasing magnetic field when $\lambda_L = \lambda_*$. At this critical point the multi-vortex state coincides with the giant vortex state and consequently there is no jump in the magnetization. But the derivatives of the coefficients C_0, C_L are discontinuous and correspondingly we expect a discontinuity in the first derivative of the magnetization. This is also confirmed by our numerical simulations where in Fig. 3 the region around the $L = 3$ multi-vortex to giant vortex transition is shown.

The magnetization of the disk $M = \int (H - H_0) d\vec{r} / 4\pi V H_{c2}$ with $R = 4.8\xi$ is shown in Fig. 4 for increasing (a) and decreasing (b) magnetic field. Jumps in the magnetization correspond to transitions between states with different number of vortices at the magnetic fields where the states cease to exist (see Fig. 1). With increasing disk thickness the demagnetization effect increases and as a result the transition points shift to larger magnetic fields, but the number of jumps remains the same. The average magnetic field in the disk can be estimated as $\langle H \rangle \approx H - 4\pi M$ and the relative magnetizations M/d as a function of $\langle H \rangle$ is ‘almost’ an universal curve for all disk thicknesses (Fig. 4(c)). For increasing magnetic field and disk thicknesses $d = 0.2, 0.4\xi$ all transitions occur between giant vortex states. For the thinner disk $d = 0.1\xi$ we observe the following sequence of transitions $0 \rightarrow 1 \rightarrow 2_g \rightarrow 3_m \rightarrow 3_g \rightarrow 4_m \rightarrow 4_g \rightarrow 5_g \rightarrow 6_g \dots$, where the lower index (g, m) corresponds to giant and multi-vortex states, respectively. For decreasing magnetic field multi-vortex states appear with a larger number of vortices. The sequence of transitions between multi-vortex states start from $L = 7$ and $L = 8$ for $d = 0.2\xi$ and $d = 0.1\xi$, respectively. For the thicker disk ($d = 0.4\xi$), a multi-vortex state appears only for $L = 3, 2$ just before the expulsion of a vortex from the disk. As is evident from Fig. 4(b), the appearance of positive magnetization observed experimentally can also be explained within the 3D GL approach without the consideration of pinning effects. But the lowest energy state, i.e. the equilibrium state, has always a negative magnetization.

To distinguish quantitatively the giant vortex state with the multi-vortex states with the same number of vortices we consider the value of the order parameter $|\Psi|^2$ in the center of the disk which is nothing else than the density of Cooper pairs. We find that this parameter, which is zero for a giant vortex state, goes almost linearly to zero when the magnetic field approaches some critical value (see Fig. 3 (a), the thick curve). Therefore, the magnetic field obtained by linearly interpolating $|\Psi(0, 0)|^2$ to zero defines the transition from a multi-vortex state to a giant vortex state. As mentioned above, our simulations show that this transition is reversible and exhibits a discontinuous derivative in the magnetization. Having the free energies of different vortex configurations we are able to construct an equilibrium vortex phase diagram which is shown in Fig. 5 for two disk radii $R = 4\xi$ and $R = 4.8\xi$, respectively. The solid curves separate the regions with different number of vortices and the dashed curves show the boundaries between the multi-vortex and the giant vortex states. For $L = 1$ the single vortex state and the giant vortex state are identical. The shaded regions correspond to the multi-vortex states. The superconducting to normal transition occurs for $H/H_{c2} \approx 1.9$ which is outside the plotted region. Notice that the multi-vortex area in the phase diagram reduces in size with increasing disk thickness and it disappears in the limit of thick disks where only the giant vortex state survives. Thus for type I superconductors

the multi-vortex state is favored with decreasing disk thickness and increasing disk radius. This behaviour can be understood as follows: with increasing radius the energy difference between different L -states decreases and consequently it becomes possible to build a lower energy multi-vortex state out of a linear combination of giant vortex states. For decreasing radius this is more difficult to do and there exists a critical radius below which no multi-vortex states have the lowest energy. To observe the multi-vortex \leftrightarrow giant vortex transition one should investigate the derivative of the magnetization or the vortex configuration itself which can be done by using e.g. a magnetic force microscope.

This work is supported by the Flemish Science Foundation (FWO-VL) through project 5.0277.97, the project INTAS-93-1495-ext and the ‘‘Interuniversity Poles of Attraction Program - Belgian State, Prime Minister’s Office - Federal Office for Scientific, Technical and Cultural Affairs’’. One of us (FMP) is a research director with the FWO-VL.

[†] Permanent address: Institute of Theoretical and Applied Mechanics, Russian Academy of Sciences, Novosibirsk 630090, Russia.

[‡] Electronic mail: peeters@uia.ua.ac.be

- [1] A.K. Geim, I.V. Grigorieva, S.V. Dubonos, J.G.S. Lok, J.C. Maan, A.E. Filippov, and F.M. Peeters, *Nature* **390**, 259 (1997).
- [2] P.S. Deo, V.A. Schweigert, F.M. Peeters, and A.K. Geim, *Phys. Rev. Lett.* **79**, 4653 (1997).
- [3] V.A. Schweigert and F.M. Peeters, *Phys. Rev. B* **58** (1 June 1998).
- [4] P.G. de Gennes, *Superconductivity of metals and alloys*, (Addison-Wesley, N.Y., 1989)
- [5] V.M. Bedanov and F.M. Peeters, *Phys. Rev. B.* **49**, 2667 (1994).
- [6] A.L. Fetter, *Phys. Rev. B* **22**, 1200 (1980).
- [7] G. Bobel, *Nuovo Cimento* **38**, 1741 (1966).
- [8] A.I. Buzdin and J.P. Brison, *Phys. Lett. A* **196**, 267 (1994).
- [9] R. Kato, Y. Enomoto, and S. Maekawa, *Phys. Rev. B* **44**, 6919 (1991).
- [10] C.P. Bean and J.B. Levingstone, *Phys. Rev. Lett.* **12**, 14 (1964).
- [11] X. Zhang and J.C. Price, *Phys. Rev. B* **55**, 3128 (1997).
- [12] V.V. Moschchalkov, X.G. Qiu, and V. Bruyndoncx, *Phys. Rev. B* **56**, 11793 (1997).

FIG. 1. The free energy of configurations with different number of vortices L for two disk radii $R = 4\xi$ (a) and $R = 4.8\xi$ (b) in the case of zero disk thickness and $\kappa = 0.28$. The open circles indicate the transition from a multi-vortex to a giant vortex state (right side of circle). The dotted curves correspond to the free energy of metastable configurations with a vortex inside a polygon for $L = 7, 8$ (b). The dashed curves are the results of our approximate analytical calculations. The insets show the possible vortex configurations.

FIG. 2. Contourplot of the magnetic field distribution in the disk plane ($z = 0$) for the case of a three vortex state and for different applied magnetic fields $H_0 = 0.525H_{c2}$ (a), $H_0 = 0.65H_{c2}$ (b), $H_0 = 0.75H_{c2}$ (c), and $H_0 = 0.8H_{c2}$ (d). We took $R = 4\xi$ and $d = 0.5\xi\kappa^2$. For the lowest magnetic field (a) the three-vortex configuration is metastable and a small decrease in the magnetic field leads to a transition to the two vortex state due to the expulsion of a vortex through the disk boundary indicated by the arrow in (a).

FIG. 3. The free energy (1), the square of the order parameter in the disk center (2), the magnetization (3), and its first derivative (4) for a disk with $R = 4\xi$, $d = 0.5\xi\kappa^2$ which is in the vortex state with $L = 3$. The dashed vertical line shows the transition from the multi-vortex state to the giant vortex state. In (a) the solid circles indicate the points at which the equilibrium phase transitions $2 \rightarrow 3$ and $3 \rightarrow 4$ occur.

FIG. 4. Magnetization of a disk in increasing (a,c) and decreasing (b) magnetic fields for $R = 4.8\xi$, $\kappa = 0.28$ and different disk radii.

FIG. 5. The vortex phase diagram for two different disk radii $R = 4\xi$ (a) and $R = 4.8\xi$ (b). The shaded area corresponds to the multi-vortex state

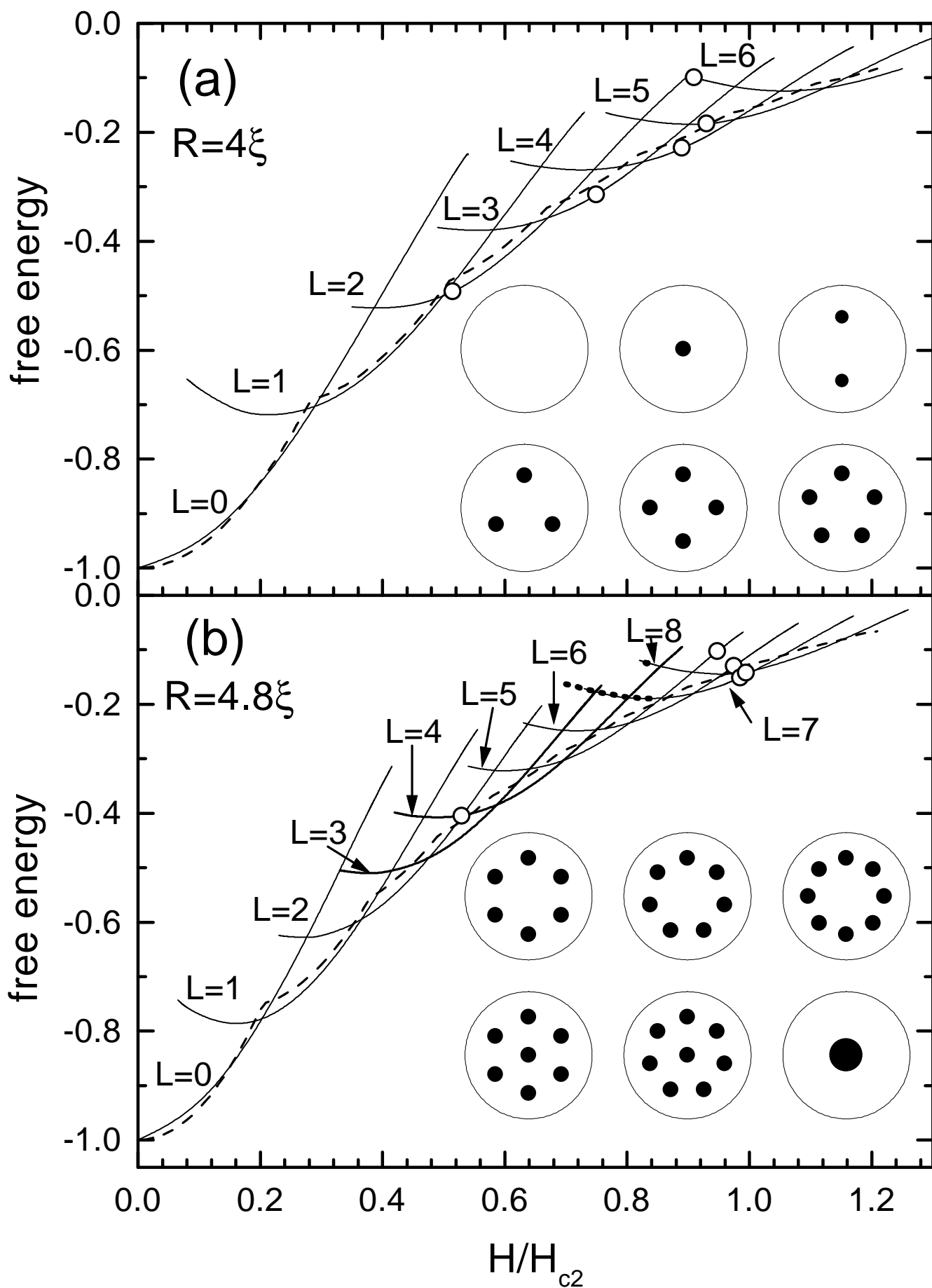


Fig.1

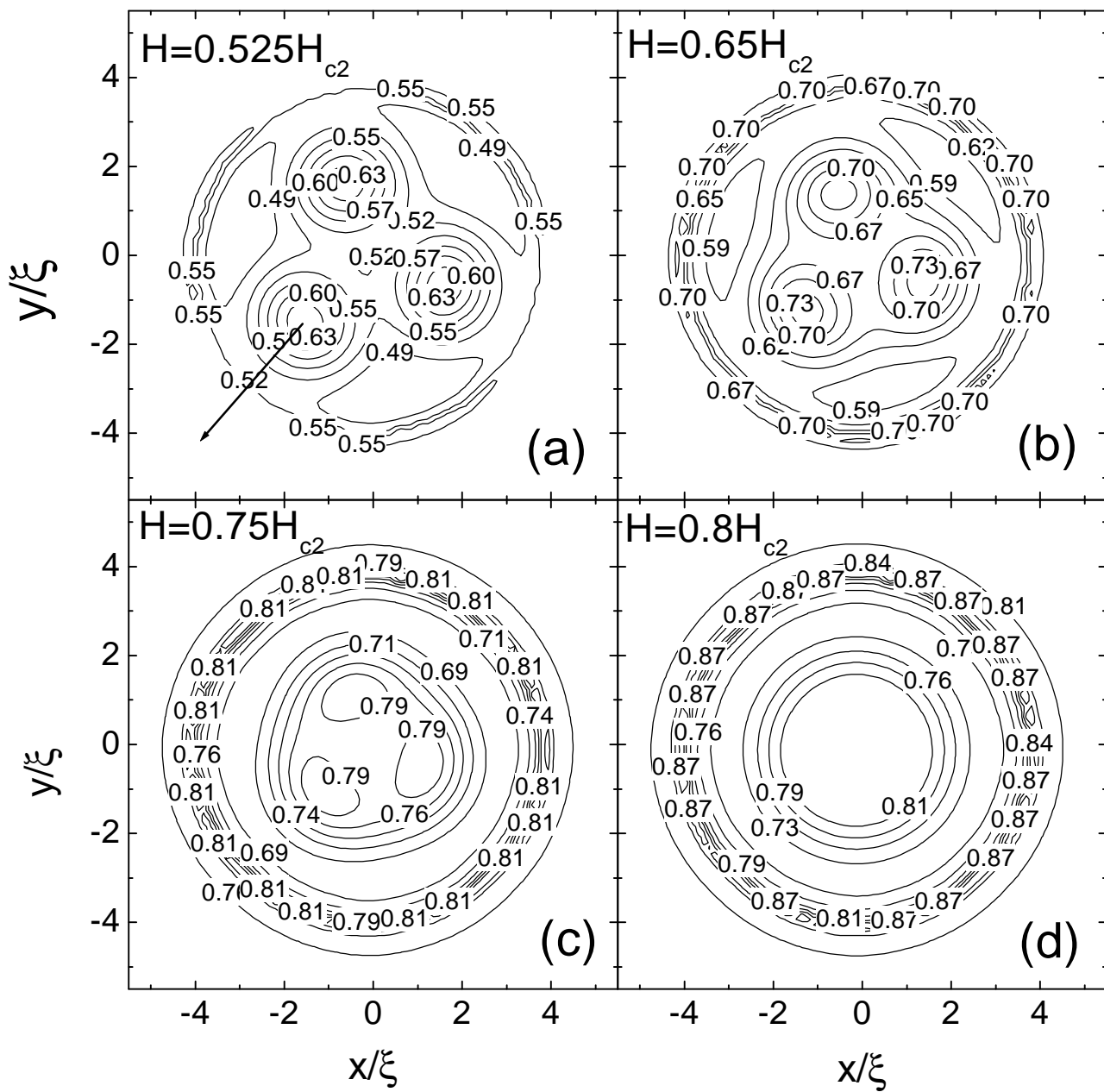


Fig.2

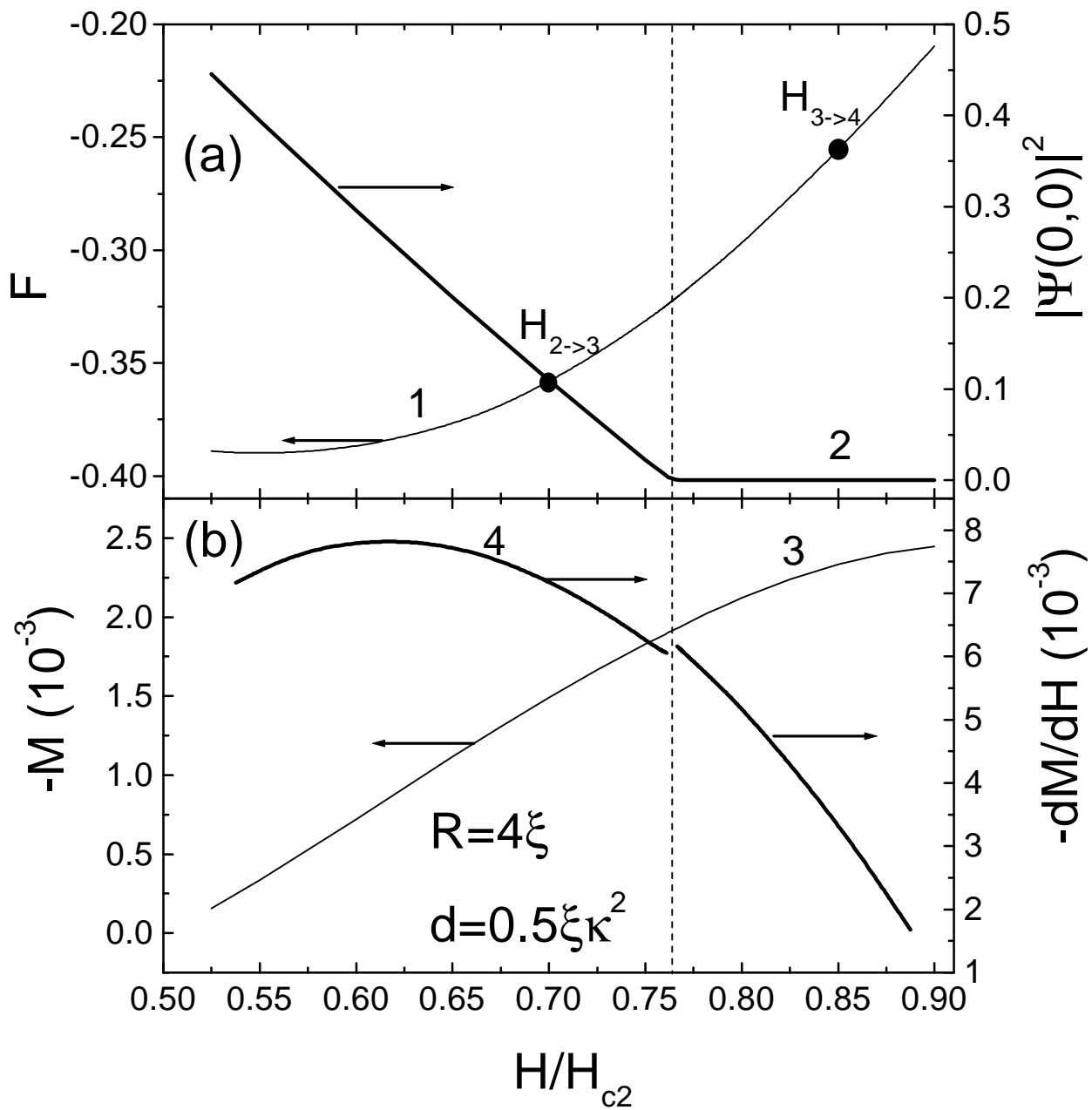


Fig.3

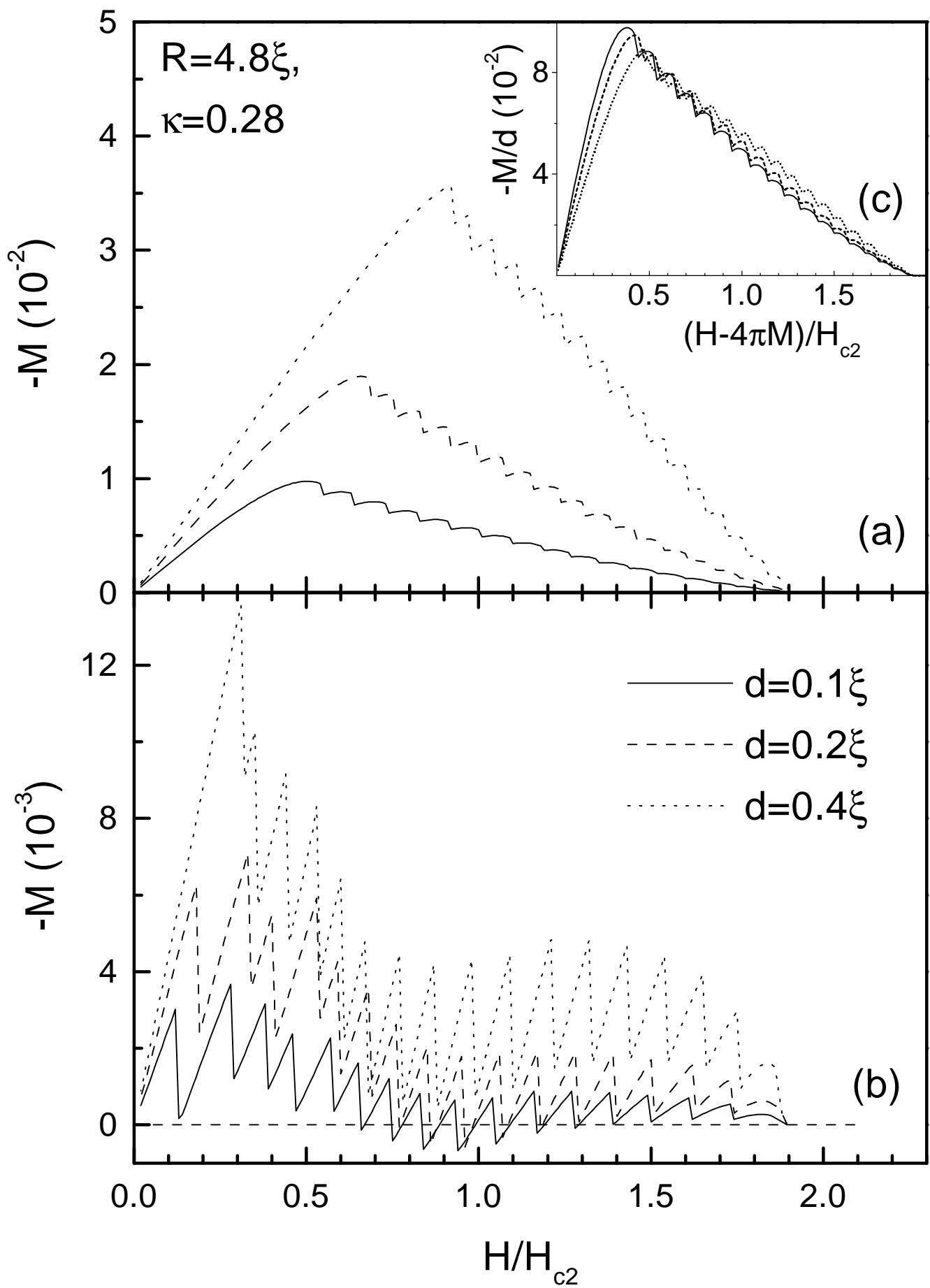


Fig.4

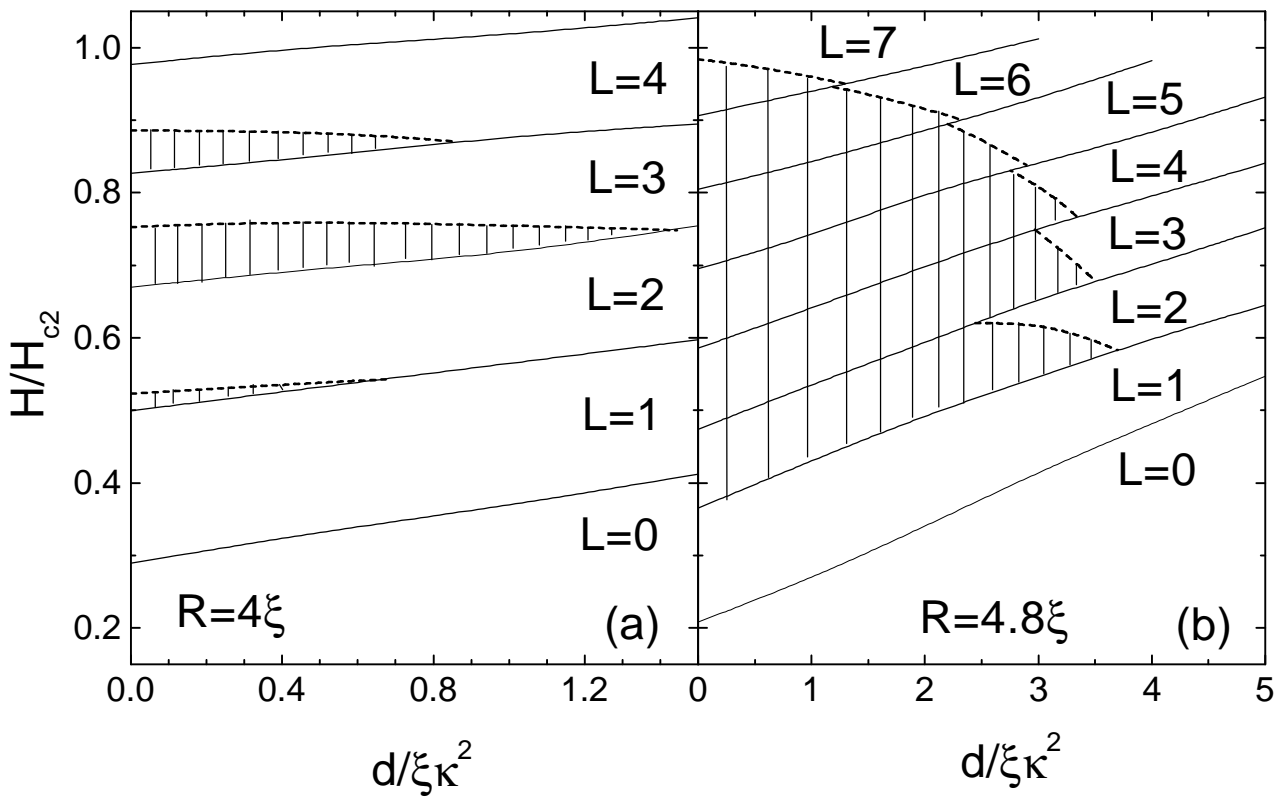


Fig.5